Spectra of jet-cooled $^{32}SO_2$ and $^{34}SO_2$ in systems $\tilde{a}\,^3B_1$ and $\tilde{b}\,^3A_2-\tilde{X}\,^1A_1$: Rotational structure of perturbed $\tilde{b}\,^3A_2$

Cheng-Liang Huang and I-Chia Chen[a)]
Department of Chemistry, National Tsing Hua University, Hsinchu, Taiwan 30013, Republic of China

Anthony J. Merer
Department of Chemistry, University of British Columbia, 2036 Main Mall, Vancouver, British Columbia V6T 1Z1, Canada

Chi-Kung Ni and A. H. Kung
Institute of Atomic and Molecular Sciences, Academia Sinica, P. O. Box 23-166, Taipei, Taiwan 106, Republic of China

(Received 21 September 2000; accepted 24 October 2000)

Spectra of $\tilde{a}\,^3B_1(\nu_1\nu_2\nu_3)=(110)$ and $(200)-\tilde{X}\,^1A_1(000)$ of $^{32}SO_2$ and $^{34}SO_2$ are obtained in a supersonic jet at a resolution 0.015 cm^{-1}. The rotational structures are analyzed for both isotopic species to obtain precise rotational and spin constants. Two new bands at 27 032.222(1) and 27 515.41(1) cm^{-1} arising from vibronic interaction separately with vibrational state (110) and (200) of $\tilde{a}\,^3B_1$ are assigned to transitions to $\tilde{b}\,^3A_2(011)$ and (101). The rotational structure of $\tilde{b}\,^3A_2$ is observed and analyzed for the first time. The two vibrational states are analyzed to yield effective rotational constants $A=1.4348(3)$, 1.89(3), $B=0.3610(3)$, 0.412(3), and $C=0.2689(3)$, 0.239(3) cm^{-1}, respectively. Then the difference $\nu_1-\nu_2$ of vibrational frequency of $\tilde{b}\,^3A_2$ is obtained to be 483.19 cm^{-1}. Because of interaction to $\tilde{b}\,^3A_2(011)$ the observed spacing of K stack and spin constants α and β for $\tilde{a}\,^3B_1(110)$ are smaller whereas the state $\tilde{a}\,^3B_1(200)$ is relatively unaffected and only spin constants vary significantly. © *2001 American Institute of Physics.*
[DOI: 10.1063/1.1333019]

I. INTRODUCTION

Spectra of sulfur dioxide in the wavelength region longer than 350 nm have been studied for several decades.[1–10] This region is assigned mainly to transition $\tilde{a}\,^3B_1-\tilde{X}\,^1A_1$. Irregular vibrational spacing is observed and explained as due to interaction with a second triplet state $\tilde{b}\,^3A_2$.[3] Hallin *et al.*[8] obtained rotationally resolved spectra for sample at dry ice temperature; they found several states at shorter wavelength to be shifted and they identified many local rotational perturbations caused by interaction with $\tilde{b}\,^3A_2$. Zen *et al.*[9] recorded the laser-induced phosphorescence spectra of isotopic variants of SO_2 and observed extra transitions in this region for isotopic species $^{16}OS^{18}O$ in solid neon. Furthermore, they assigned this extra progression as $\tilde{b}\,^3A_2-\tilde{X}\,^1A_1$ and determined the false origin $\tilde{b}\,^3A_2(001)$ to be 26 653 cm^{-1}. Near band origin, previous work[10] on bands to vibrational levels $\tilde{a}\,^3B_1(010)$ and (100) with high resolution for SO_2 in supersonic jet indicates no interaction with nearby $\tilde{b}\,^3A_2$ for states with low rotational quantum numbers. However, in the rotational states $K=5$ and 6 of (100), perturbations were reported by Brand *et al.*[3] Consequently, deviation in rotational constant B determined from states with K equal to 5 and 6 is reported from the value obtained from states with low K.

Our spectra of sulfur dioxide in a supersonic jet to decrease spectral congestion enable us to differentiate weak bands and to assign rovibronic transitions to a triplet state other than $\tilde{a}\,^3B_1$. In this work a preliminary survey showed that near transitions $\tilde{a}\,^3B_1(110)$ and $(200)-\tilde{X}\,^1A_1(000)$ two new bands appear, possibly involving $\tilde{b}\,^3A_2$, encouraging subsequent spectra at high resolution. We report results of analyses of full spin and rotational structure of bands to levels $\tilde{a}\,^3B_1(110)$ and (200) and to two new states. These results allow us to assign definitely these new vibrational states to be $\tilde{b}\,^3A_2$ and to investigate the effect of interaction between these two triplet states. The results of theoretical calculations[11] indicate three triplet states $^3B_1$, $^3A_2$, and $^3B_2$ in the UV region that can interact with one another. In study of dissociation dynamics of SO_2, an alternative pathway via intersystem crossing to a triplet state leading to products is suggested at photolysis wavelength near 193 nm.[12] Hence understanding the spectroscopy in near UV region is important in identifying these triplet states and interaction mechanisms among them.

II. EXPERIMENTAL DETAILS

A. Medium resolution

Sulfur dioxide seeded in helium or argon around 1%–15% was expanded through an orifice (diameter 0.5 mm) to obtain the molecular jet. A pulsed valve was piezoelectrically actuated at 10 Hz and the voltage of controller (Physik

[a)]Author to whom correspondence should be addressed; electronic mail: icchen@mx.nthu.edu.tw

Instrumente P-270) was set at 700–800 V. The stagnation pressure behind nozzle was kept about 2.5 atm.

A tunable UV laser was obtained on mixing pulses at 1064 nm from a seeded Nd:YAG laser (Continuum NY 81C) with output of a dye laser (Continuum ND 60) in a KDP crystal (INRAD M3). Several dyes (DCM, R6G, and F548) were used to generate the UV beam in the wavelength region 360–390 nm. The energy of UV pulses was 3–5 mJ/pulse. This UV beam intersected the molecular jet about 2 cm beyond the nozzle. Emission of SO_2 was detected with a photomultiplier (Hamamatsu R928) after passing a color filter (GG385) and an interference filter (400 ± 10 nm). The signal was sent to a gated integrator with gate width about 15 μs. Most spectra were recorded when the pulsed nozzle was mounted in a direction such that the molecular jet was moving toward the detector. Under this condition, emission with long decay was observed. The linewidth of SO_2 spectra is measured to be 0.06–0.1 cm^{-1}; this magnitude resulted from a combination of laser linewidth and Doppler velocity spread of the molecular jet.

We calibrated the absolute frequency with combination of optogalvanic lines of neon and I_2 transitions to within ±0.02 cm^{-1}. The wavelength of the seeded YAG laser was determined first on several days to verify the stability of absolute position of the seeder; within the period of measurements, variation of frequency of the seeder was much less than 0.01 cm^{-1}. Hence, the absolute frequency of the UV laser was determined on adding the frequency of the visible beam to the fundamental frequency of the YAG beam.

B. High resolution

The experiments at high resolution were performed as described elsewhere,[10,13,14] and are summarized as follows. A cw ring laser (Coherent 699/29, dye R6G) pumped with an Ar^+ laser (Coherent) served to generate the seeding beam. An amplifier containing three stages of dye cells pumped with a Nd:YAG laser was used to amplify this seeding beam. The output of this amplifier was mixed in a KDP crystal (INRAD M3) with output of a seeded Nd:YAG laser to generate pulses at 363–380 nm. Total emission of SO_2 was collected through a spatial filter to decrease the spectral full width at half maximum (FWHM) intensity to 0.015–0.02 cm^{-1} from Doppler spread. A photon counter counted the signal with a counting interval of 150 μs. About 60–100 laser shots were averaged for each data point.

We have calibrated the high-resolution spectra with the transitions of SO_2 recorded with medium resolution. The detailed procedure of the calibration is described elsewhere.[10] With this method the accuracy of absolute frequency is ±0.02 cm^{-1}. For high-resolution work the uncertainty is mainly attributed to broad features of optogalvanic neon lines. The precision of relative positions is expected to be within 0.002 cm^{-1}.

III. RESULTS AND DISCUSSION

A. State $\tilde{a}\,^3B_1$

A survey scan in the wavelength region 350–385 nm of sulfur dioxide appears in Fig. 1. New bands near the blue end

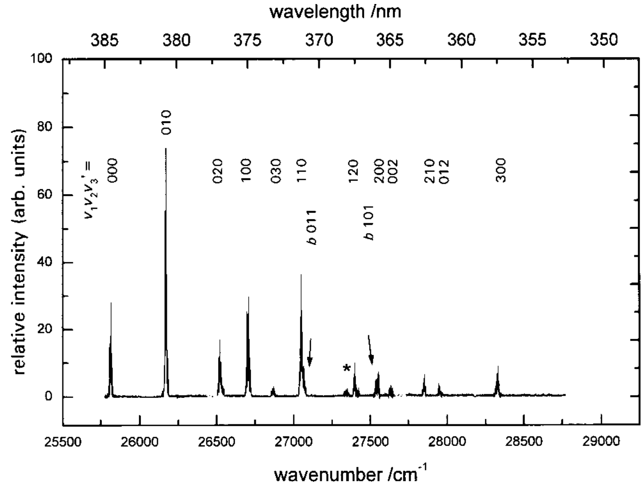

FIG. 1. Survey spectrum of the $\tilde{a}\,^3B_1-\tilde{X}\,^1A_1$ system of SO_2 in the wavelength region 350–385 nm. (v_1,v_2,v_3') denotes an assignment for a vibrational level of $\tilde{a}\,^3B_1$ and $b(011)$ and $b(101)$ for vibrational levels of $\tilde{b}\,^3A_2$. An asterisk denotes band near transition $\tilde{a}\,^3B_1(120)-\tilde{X}\,^1A_1(000)$ possibly belonging to $\tilde{b}\,^3A_2$.

of transition $\tilde{a}\,^3B_1(110)-\tilde{X}\,^1A_1(000)$ and the red end of (200)–(000), recorded at medium resolution, are shown in Figs. 2 and 3, respectively. The branch notation used in these figures is $^{\Delta K}\Delta J_{F_i'}$, where the spin component label F_i',

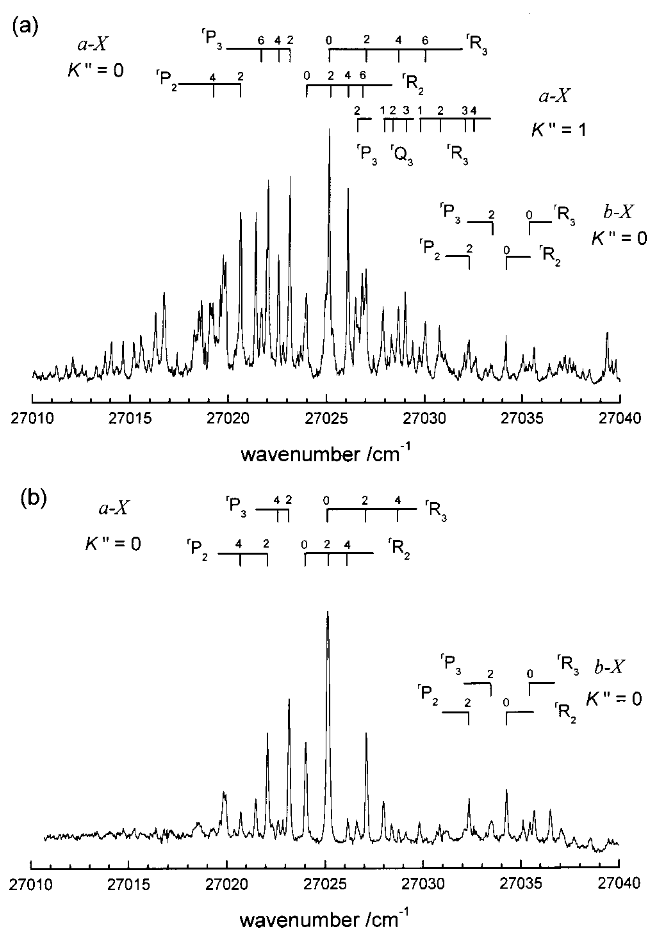

FIG. 2. Medium-resolution spectra of $\tilde{a}\,^3B_1(110)$ and $\tilde{b}\,^3A_2(011)-\tilde{X}\,^1A_1(000)$ with seeding ratio (a) 5% and (b) 1% of SO_2 in helium and stagnation pressure 2.5 atm.

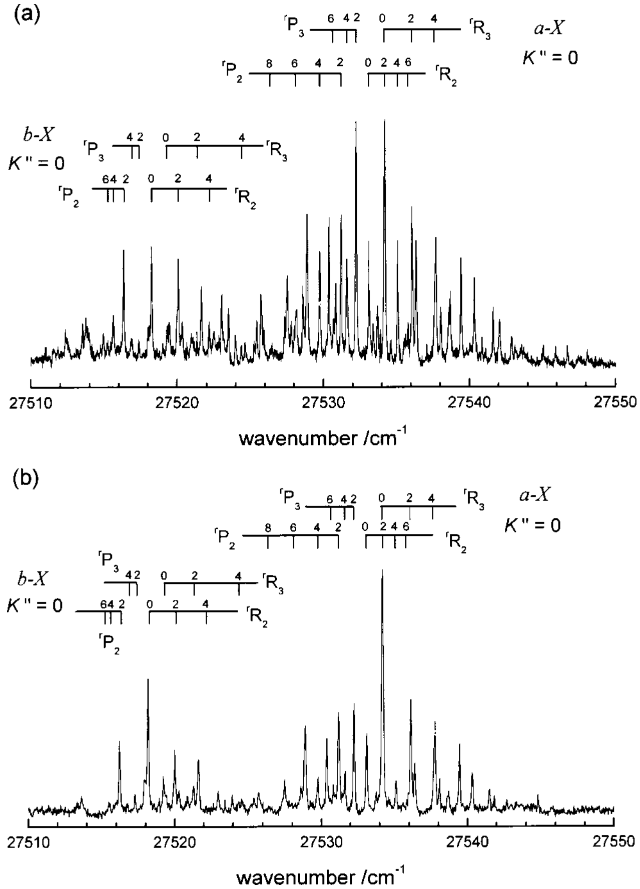

FIG. 3. Medium-resolution spectra of $\tilde{a}\,^3B_1(200)$ and $\tilde{b}\,^3A_2(101)-\tilde{X}\,^1A_1(000)$ with seeding ratio (a) 5% and (b) 1% of SO_2 in helium and stagnation pressure 2.5 atm.

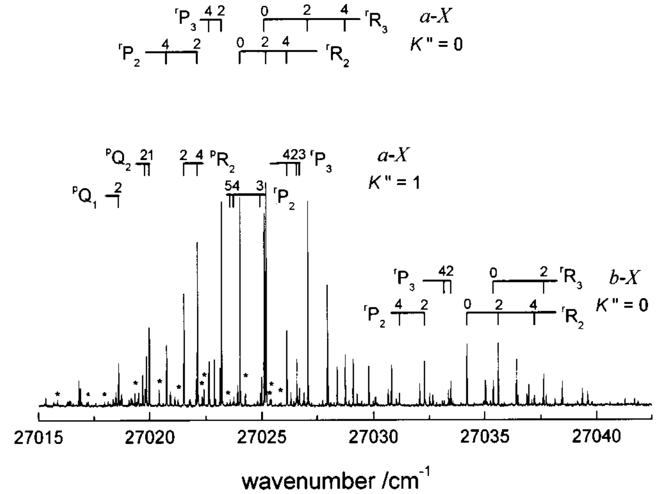

FIG. 4. High-resolution spectrum of bands $\tilde{a}\,^3B_1(110)$ and $\tilde{b}\,^3A_2(011)-\tilde{X}\,^1A_1(000)$ of SO_2. A line marked with an asterisk is assigned to $^{34}SO_2$.

$i=1$–3 indicates levels with $J=N+1$, N and $N-1$, respectively. With decreased seeding ratio of SO_2 in helium, the relative spectral intensity of these transitions increases indicating that those lines must be from low rotational states. Experiments at high resolution enable resolution of congested lines in these two bands and investigation of interaction between perturbed states. Spectra in the region of bands to levels (110) and (200) at resolution 0.015 cm^{-1} appear in Figs. 4–7, separately. The spectrum shown for (200) was recorded at a seeding ratio greater than that for (110) to improve the ratio of signal to noise; hence we expect a rotational temperature warmer than that for spectrum (110) shown here. For Figs. 4–7 no correction for intensity fluctuation of the excitation laser was performed. However, taking into account the laser intensity, we estimated the ratio of spectral intensity of the new band to that of band (200) on comparing the most intense peaks to be about 1:3.

The rotational structure of bands to $\tilde{a}\,^3B_1(110)$ and (200) is similar to that of bands to vibrational levels (100) and (010). The detailed description about the rotational structure of SO_2 single–triplet transition has been described previously.[1–3,10] We reported the performed full spin and rotational analysis on the latter two bands,[10] and assignments for the present bands were made accordingly. The experimentally observed positions are presented in Tables I and II of Ref. 15 for transitions to states $\tilde{a}\,^3B_1(110)$ and (200), respectively. Some remaining weak lines forming similar rotational structure are assigned to be $^{34}SO_2$ for both bands. Transitions belonging to $^{34}SO_2$ are marked with asterisks and are shown in Figs. 4, 6, and 7; their positions are listed in Tables III and IV of Ref. 15.

After assignment of transitions to states (110) and (200) for both isotopes, the remaining lines are expected to belong to new bands. The rotational structures of both new bands display a *c*-type pattern similar to that in system $\tilde{a}\,^3B_1$; hence the selection rules applied are expected to be the same. As spectra were recorded at high resolution, knowledge of precise rotational levels of the ground electronic state[4,16] enables most lines in perturbed bands to be assigned. After completing the assignments, we found that, for both new bands, transitions to F_2 components are much more intense than to F_3 components, in contrast to the $\tilde{a}\,^3B_1$ system.[10,17] The F_2 lines in the new system are enhanced via interaction to $\tilde{a}\,^3B_1$. Figures 5 and 7 show spectra and assignments of new bands; Tables V and VI of Ref. 15 list the rotational assignments to two new states. Because of an excellent signal to noise ratio, we were able to assign some very weak transitions to isotopic species $^{34}SO_2$ for the new band near (200); Table VII of Ref. 15 presents transitions and assignments. Transitions of $^{34}SO_2$ for the band near (110) are too weak for us to obtain enough lines to form a band.

Even though these states are perturbed, the program ASYTOP[18,19] was used to perform successive refinements to yield best-fit rotation and spin constants (defined by Sears[18,19]). Effective rotational and spin constants from results of least-squares fits as well as rms are summarized in Tables I and II. Deviation of position calculated with these constants from the observed value is listed in Tables I–V of Ref. 15. For state $\tilde{a}\,^3B_1(200)$ the average deviation between calculated and observed positions is smaller than that for level $\tilde{a}\,^3B_1(110)$. The rms for the latter level is significantly greater than experimental uncertainty, resulting from interaction with the nearby level. The level $\tilde{a}\,^3B_1(200)$ seems not to

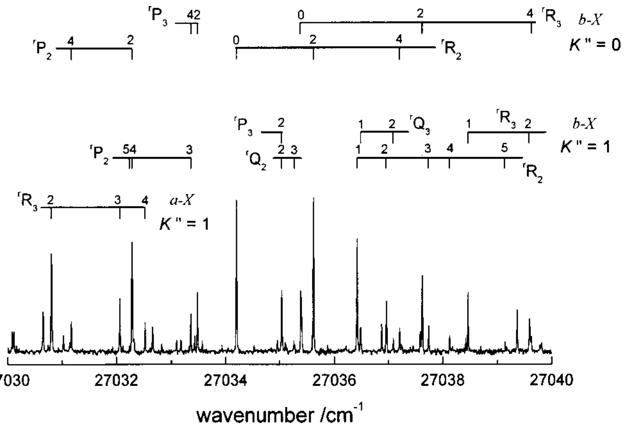

FIG. 5. The enlarged part of Fig. 4 for the transition $\tilde{b}\,^3A_2(011)-\tilde{X}\,^1A_1(000)$ of SO_2.

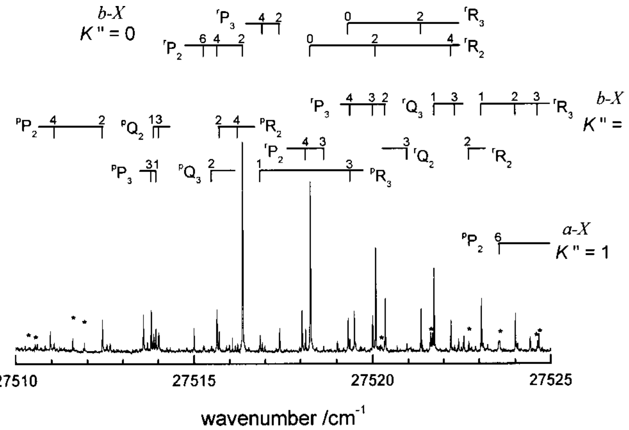

FIG. 7. The enlarged part of Fig. 6 for the transition $\tilde{b}\,^3A_2(101)-\tilde{X}\,^1A_1(000)$ of SO_2. A line marked with an asterisk is assigned to $^{34}SO_2$.

be affected by its nearby state except that the spin constant α becomes smaller than those in $\tilde{a}\,^3B_1(000)$.

B. State $\tilde{b}\,^3A_2$

For the new level near (110) several transitions to states $K'=1$ and 2 were observed whereas only two transitions to a $K'=0$ state ($N_{KaKc}=1_{01}$, F_2) were assigned; other states may not interact with state (110) to show observable intensity. On the basis of these observed transitions the least-squares fits show a rms deviation of 0.010 cm^{-1}, which is 2–3 times of those for the $\tilde{a}\,^3B_1$. Several transitions to $K'=0-2$ are observed and assigned for the new level near (200), but the calculated positions deviate significantly, precluding reasonable effective rotational constants. However, the effect of perturbation from this new state onto the state $\tilde{a}\,^3B_1(200)$ is insignificant.

We plotted the observed term value versus $N(N+1)$ to show relative positions of these perturbing states. Figure 8 shows plots for $\tilde{a}\,^3B_1(100)$, (110), (200) and two new states. Here, level (100) is unaffected by the nearby triplet state shown previously,[10] and is shown here for comparison. From these plots for state $\tilde{a}\,^3B_1(110)$ the spacings among $K'=0$, 1, and 2 are smaller than those for other states whereas level $\tilde{a}\,^3B_1(200)$ displays normal spacing. Hence, for level $\tilde{a}\,^3B_1(110)$ the constant A obtained from low K states, affected significantly by interaction with the nearby state, is much smaller than that in $\tilde{a}\,^3B_1(000)$.

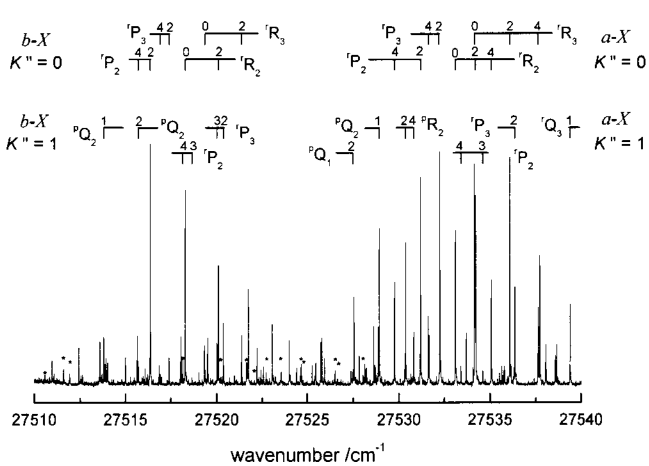

FIG. 6. High-resolution spectrum of $\tilde{a}\,^3B_1(200)$ and $\tilde{b}\,^3A_2(101)-\tilde{X}\,^1A_1(000)$ of SO_2. A line marked with an asterisk is assigned to $^{34}SO_2$.

Compared with those for $\tilde{a}\,^3B_1$, the spacings among K stacks of these two new vibrational levels are small. In addition, a relatively large splitting is observed between the upper and lower states of K doublet for $K'=1$; this normally indicates a large difference in effective rotational constants B and C. Because the rotational constants of level near (200) cannot be evaluated with a least-squares fit we estimated their values as follows. Assuming that splitting purely from spin interaction between F_2 and F_3 states is small, we express for an asymmetric rotor the rotational energy E_r of upper and lower states of $K=1$ as

$$\text{upper state:}\quad E_r=N(N+1)((3/4)B+(1/4)C)+(A-B), \tag{1}$$

$$\text{lower state:}\quad E_r=N(N+1)((1/4)B+(3/4)C)+(A-B). \tag{2}$$

From slopes of upper and lower states of $K=1$ doublets versus $N(N+1)$ in Fig. 8(c) we estimate effective rotational constants $B=0.412(3)$ and $C=0.239(3)\ cm^{-1}$ for the new level near (200). As the spacing of K stack is $\propto(A-B)$, we estimated constant A to be 1.89(3) cm^{-1} from spacing between $K=0$ and 2.

According to data obtained from experiments with solid neon,[9] with account taken of the matrix shift 18 cm^{-1}, the transition to state $\tilde{a}\,^3B_1(011)$ is expected to lie about 27 053 cm^{-1}, and that to state (050) about 27 544 cm^{-1}. The intensity of the band to (011) is expected to be negligible under the experimental conditions; for the transition to (050) the Franck–Condon factor is small, but bands to these states might gain intensity from mixing with nearby bright states. However, these states are expected to have a rotational constant A larger than or comparable to that in the vibrational ground state, contrary to the experimental results. That these two new bands display similar spectral intensity and rotational constants B and C implies that they are from the same electronic state.

TABLE I. Rotational and spin constants[a] (cm^{-1}) of $^{32}SO_2$ and $^{34}SO_2$ $\tilde{a}\,^3B_1$.

	$^{32}SO_2\ \tilde{a}\,^3B_1(000)$[b]	$^{32}SO_2\ \tilde{a}\,^3B_1(110)$	$^{32}SO_2\ \tilde{a}\,^3B_1(200)$	$^{34}SO_2\ \tilde{a}\,^3B_1(110)$	$^{34}SO_2\ \tilde{a}\,^3B_1(200)$
T_0	25 765.737(2)	27 021.596(1)	27 530.574(1)	27 018.810(1)	27 521.050(1)
A	2.313 053(73)	2.030 4(9)[c]	2.213 0(3)	2.0493(12)	2.1552(6)
B	0.297 179(9)	0.315 84(15)	0.306 39(3)	0.3174(3)	0.3066(3)
C	0.262 511(9)	0.262 86(15)	0.260 96(3)	0.2594(3)	0.2601(3)
$\Delta_K/10^6$	290.09(90)	⋯	⋯	⋯	⋯
$\Delta_{JK}/10^6$	−7.889(52)	⋯	⋯	⋯	⋯
$\Delta_J/10^6$	0.241 2(23)	⋯	⋯	⋯	⋯
$\delta_K/10^6$	2.17(38)	⋯	⋯	⋯	⋯
$\delta_J/10^6$	0.057 6(20)	⋯	⋯	⋯	⋯
α	0.107 0(11)	0.028 6(12)	0.044 1(9)	0.0222(18)	0.0374(27)
β	−0.027 8(11)	−0.018 5(24)	−0.009 6(12)	−0.026 (6)	−0.0616(81)
ϵ_{aa}	0.021 01	0.062 2(24)	0.028 9(6)	0.028 9[d]	0.0289[d]
ϵ_{bb}	−0.001 297	−0.020 6(18)	−0.003 8(6)	0.0[e]	0.0[e]
ϵ_{cc}	−0.003 144	−0.022 4(18)	−0.004 8(6)	0.0[e]	0.0[e]
rms		0.024 2	0.005 7	0.0078	0.0028

[a]Uncertainties (3σ) are in units of the last significant figure.
[b]Ground-state constants of both isotopic species are taken from Belov *et al.* (Ref. 16) and those of $^{32}SO_2\ \tilde{a}\,^3B_1(000)$ from Hallin *et al.* (Ref. 4).
[c]Small A value results from interaction to $\tilde{b}\,^3A_2(011)$.
[d]The parameter is fixed to the value of $^{32}SO_2\ \tilde{a}\,^3B_1(200)$ during least-squares fits.
[e]The parameter is set to zero during least-squares fits.

Hallin *et al.*[8] and Zen *et al.*[9] assigned some vibronic transitions to state $\tilde{b}\,^3A_2$ that arise from interaction to $\tilde{a}\,^3B_1$. Comparing all the experimental results we assign these two bands at 27 032.222(1) and 27 515.41(1) cm^{-1} to be transitions to $\tilde{b}\,^3A_2(011)$ and (101), respectively. Our experimental data with such a small A constant agree with the results of *ab initio* calculations that yield an angle O–S–O of $\tilde{b}\,^3A_2$ to be 90°–100°;[11,20] a small O–S–O angle means a small rotational constant A. On the basis of fitted rotational constants of $\tilde{b}\,^3A_2(011)$ and (101) the bond distance of S–O is calculated to be 1.476 and 1.35 Å and angle O–S–O 109° and 113°, respectively. As the extent of interaction varies this geometry obtained is expected to differ. The angle O–S–O of unperturbed level of $\tilde{b}\,^3A_2$ is expected to be smaller than the experimental values obtained in this work.

An isotopic shift of 9.29 cm^{-1} for state $\tilde{b}\,^3A_2(101)$ also agrees with our vibrational assignment; for (050) the shift is expected to be greater than about 12 cm^{-1}, according to the results from solid neon and this work. In addition, our assignments agree with the results of Hallin *et al.*[4] that indicate $\tilde{b}\,^3A_2$ interacting with $\tilde{a}\,^3B_1$ at low rotational states near levels (110) and (200).

TABLE II. Rotational and spin constants[a] (cm^{-1}) of $\tilde{b}\,^3A_2$ of $^{32}SO_2$ and $^{34}SO_2$.

	$^{32}SO_2\ \tilde{b}\,^3A_2(011)$	$^{32}SO_2\ \tilde{b}\,^3A_2(101)$	$^{32}SO_2\ \tilde{b}\,^3A_2(101)$
T_0	27 032.222(1)	27 515.41(1)	27 506.12(5)
A	1.4348(3)	1.89(3)	1.85(9)
B	0.3610(3)	0.412(3)	0.406(6)
C	0.2689(3)	0.239(3)	0.251(6)
α	−0.0184(15)		
β	−0.069(6)		
ϵ_{aa}	−0.0507(12)		
ϵ_{bb}	−0.0325(12)		
ϵ_{cc}	−0.0525(12)		
rms	0.010		

[a]Uncertainties (3σ) are in units of the last significant figure.

Because the two new bands belong to a c-type transition, the symmetry of vibrational level is assigned to be b_2,[2] implying odd vibrational quanta in vibrational mode ν_3. On the basis of the false origin of $\tilde{b}\,^3A_2(001)$ for $^{16}OS^{18}O$ to be 26 653 cm^{-1} proposed by Zen *et al.*,[9] we assign the vibrational quantum number $\nu_3 = 1$ for these new states. Then, the difference of vibrational frequency $\nu_1 - \nu_2$ for $\tilde{b}\,^3A_2$ is calculated to be 483.19 cm^{-1}. Compared with the value 476 cm^{-1} obtained from solid neon[9] for isotopic species $^{16}OS^{18}O$ the vibrational ratio of these isotopic species agrees with that for the $\tilde{a}\,^3B_1$ system.

The third triplet state $^3B_2$ has a calculated equilibrium O–S–O angle near 110° and could be the perturber. However its vibronic symmetry is b_2 and a_1 different from that of $\tilde{a}\,^3B_1(110)$ and (200) and should not interact with each other via vibronic coupling. In addition, via the spin–orbit coupling $^3B_2$ is expected to have an a-type transition different from this experimental finding.

From the results of least-squares fits, the spin constants α, β and spin-rotation constant ϵ for levels $\tilde{a}\,^3B_1(110)$ and (200) vary widely from interaction with $\tilde{b}\,^3A_2$. The results show that interacting with $\tilde{b}\,^3A_2$ causes decreased splitting from spin–spin interaction. Because the energy separation of perturbing states decreases, the spin-rotation constants are expected to increase. Overall the perturbed vibrational levels of $\tilde{b}\,^3A_2$ have small spin constants and large values of ϵ. Both levels have the same rovibronic symmetry as those of the $\tilde{a}\,^3B_1$ state; we conclude that these two vibrational levels of $\tilde{b}\,^3A_2$ arise from vibronic interaction with the $\tilde{a}\,^3B_1$ state.

About seven transitions are assigned to $\tilde{b}\,^3A_2(101)$ for isotopic species $^{34}SO_2$. We obtained rotational constants A, B, and C using Eqs. (1) and (2) and list them in Table II. The

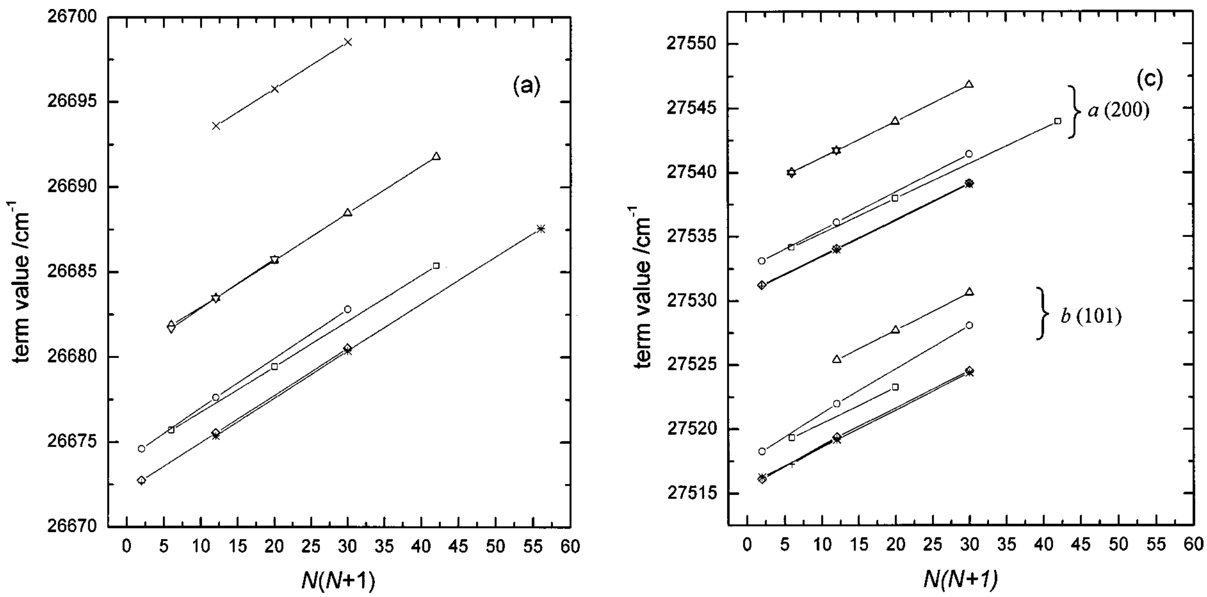

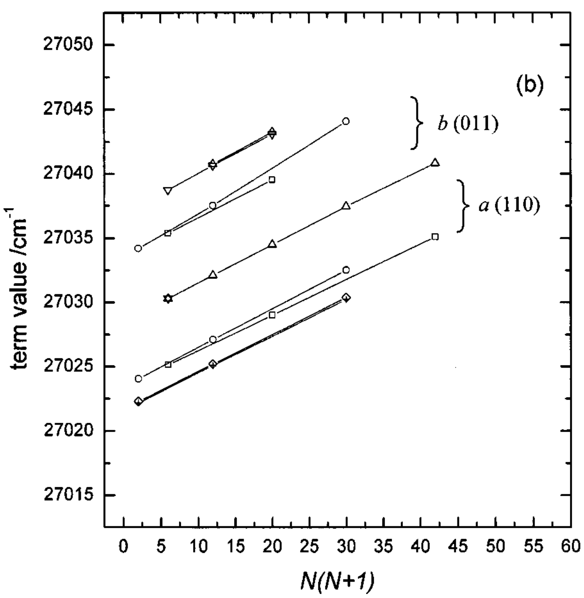

FIG. 8. Plots of measured term values vs $N(N+1)$ obtained from high-resolution spectra for (a) $\tilde{a}\,^3B_1(100)$, (b) $\tilde{a}\,^3B_1(110)$ and $\tilde{b}\,^3A_2(011)$, and (c) $\tilde{a}\,^3B_1(200)$ and $\tilde{b}\,^3A_2(101)$. The symbols $+$, $\diamond$, $*$, $\bigcirc$, $\square$, $\bigtriangledown$, $\triangle$, $\times$ denote $K'=0, F_1$, F_2, and F_3, $K'=1, F_2$, and F_3, $K'=2, F_2$, and F_3, and $K'=3$, F_3 states, respectively.

band origin for $^{34}SO_2$ is then determined to be at 27 506.12(5) cm^{-1}.

IV. SUMMARY

Spectra near bands $\tilde{a}\,^3B_1(110)$ and $(200)-\tilde{X}\,^1A_1(000)$ of $^{32}SO_2$ and $^{34}SO_2$ were recorded in a supersonic jet at resolution 0.015 cm^{-1}. Two new bands at 27 032.222(1) and 27 515.41(1) cm^{-1} are assigned to be transitions to $\tilde{b}\,^3A_2(011)$ and (101), respectively. Then, the difference of vibrational frequency $\nu_1-\nu_2$ is obtained to be 483.19 cm^{-1}. The rotational structure of bands to state $\tilde{b}\,^3A_2$ is observed for the first time and is analyzed to yield effective rotational constants. These two bands appear because of vibronic interaction to nearby vibrational levels of $\tilde{a}\,^3B_1$. Only two triplet states are observed in the wavelength region longer than 350 nm. The lines belonging to transitions to $\tilde{b}\,^3A_2(101)$ of $^{34}SO_2$ are assigned.

To the red of the band $\tilde{a}\,^3B_1(120)-\tilde{X}\,^1A_1(000)$ a new band appearing with medium intensity, shown in Fig. 1, is assigned not to the $\tilde{a}\,^3B_1$ system but on the basis of results of previous[8,9] and of this work, to state $\tilde{b}\,^3A_2$. From the survey scan, the relative intensity indicates strong interaction between this state and $\tilde{a}\,^3B_1(120)$. Future work using a laser with high resolution in this region can provide information on separation among various vibrational states of $\tilde{b}\,^3A_2$ and more detailed information on interaction of these two triplet states.

ACKNOWLEDGMENTS

C.-L.H. and I-C.C. thank the National Science Council of the Republic of China for financial support under Contract No. NSC 88-2113-M-007-045. C.K.N. and A.H.K. thank NSC and China Petroleum, Taiwan for their partial support. We thank the Ministry of Education, Taiwan for support of this cooperative research between Canada and Taiwan.

[1] A. J. Merer, Discuss. Faraday Soc. **35**, 127 (1963).
[2] J. C. D. Brand, V. T. Jones, and C. di Lauro, J. Mol. Spectrosc. **40**, 616 (1971).
[3] J. C. D. Brand, V. T. Jones, and C. di Lauro, J. Mol. Spectrosc. **45**, 404 (1973).
[4] K. E. J. Hallin, Y. Hamada, and A. J. Merer, Can. J. Phys. **54**, 2118 (1976).
[5] F. Hegazi, F. Al-Adel, A. Hamdan, and A. Dastageer, J. Phys. Chem. **98**, 12169 (1994).
[6] J. S. Baskin, F. Al-Adel, and A. Hamdan, Chem. Phys. **200**, 181 (1995).
[7] J. A. Joens, Chem. Phys. Lett. **261**, 659 (1996).
[8] K. E. J. Hallin, Y. Hamada, and A. J. Merer (unpublished).
[9] C.-C. Zen, Y. P. Lee, I-C. Chen, and A. J. Merer, J. Phys. Chem. A **104**, 771 (2000).
[10] C.-L. Huang, S.-S. Ju, I-C. Chen, A. J. Merer, C. K. Ni, and A. H. Kung, J. Mol. Spectrosc. **203**, 151 (2000).
[11] H. Katagiri, T. Sako, A. Hishikawa, T. Yazaki, K. Onda, K. Yamanouchi, and K. Yoshino, J. Mol. Struct. **413–414**, 589 (1997).
[12] P. C. Ray, M. F. Arendt, and L. J. Butler, J. Chem. Phys. **109**, 5221 (1998).
[13] C. K. Ni and A. H. Kung, Opt. Lett. **21**, 1673 (1996).
[14] C. K. Ni and A. H. Kung, Appl. Opt. **37**, 530 (1998).
[15] See EPAPS Document No. E-JCPSA6-114-009104 for seven tables of lists of observed and deviation from calculated line positions of $^{34,32}SO_2$ $\tilde{a}\,^3B_1$ and $\tilde{b}\,^3A_2$. This document may be retrieved via the EPAPS homepage (http://www.aip.org/pubservs/epaps.html) or from ftp.aip.org in the directory /epaps/. See the EPAPS homepage for more information.
[16] S. P. Belov, M. Y. Tretyakov, I. N. Kozin, E. Klisch, G. Winnewisser, W. J. Lafferty, and J.-M. Flaud, J. Mol. Spectrosc. **191**, 17 (1998).
[17] J. T. Hougen, Can. J. Phys. **42**, 433 (1963).
[18] T. J. Sears, Comput. Phys. Rep. **2**, 1 (1984).
[19] T. J. Sears, Comput. Phys. Commun. **34**, 123 (1984).
[20] H. F. Schaeffer (unpublished).